

Implications of Mini-EUSO measurements for a space-based observation of UHECRs

Mario Bertaina^{a,b,*}, Matteo Battisti^{b,i}, Marta Bianciotto^{a,b}, Karl Bolmgren^j and Francesco Fenu^{p,m} for the JEM-EUSO Collaboration

(a complete list of authors can be found at the end of the proceedings)

^aUniversity of Turin, Department of Physics, V. P. Giuria 1, 10125 Turin, Italy

^bINFN Section of Turin, Via P. Giuria 1, 10125 Turin, Italy

ⁱUniv. Paris Cité, CNRS, Astroparticule & Cosmologie, 10 Rue A. Domon & L. Duquet, 75013 Paris, France

^jKTH Royal Institute of Technology, Brinellvägen 8, 114 28 Stockholm, Sweden

^mASI, Italian Space Agency, Via del Politecnico, 00133 Rome, Italy

^pKIT, Hermann-von-Helmholtz-Platz 1, 76344 Eggenstein-Leopoldshafen, Germany

E-mail: bertaina@to.infn.it

Mini-EUSO is the first mission of the JEM-EUSO program on board the International Space Station. It was launched in August 2019 and it is operating since October 2019 being located in the Russian section (Zvezda module) of the station and viewing our planet from a nadir-facing UV-transparent window. The instrument is based on the concept of the original JEM-EUSO mission and consists of an optical system employing two Fresnel lenses of 25 cm each and a focal surface composed of 36 Multi-Anode Photomultiplier tubes, 64 channels each, for a total of 2304 channels with single photon counting sensitivity and an overall field of view of $44 \times 44^\circ$. Mini-EUSO can map the night-time Earth in the near UV range (predominantly between 290 nm and 430 nm), with a spatial resolution of about 6.3 km and different temporal resolutions of 2.5 μ s, 320 μ s and 41 ms. Mini-EUSO observations are extremely important to better assess the potential of a space-based detector in studying Ultra-High Energy Cosmic Rays (UHECRs) such as K-EUSO and POEMMA. In this contribution we focus the attention on the results of the UV measurements and we place them in the context of UHECR observations from space, namely the estimation of exposure.

38th International Cosmic Ray Conference (ICRC2023)
26 July - 3 August, 2023
Nagoya, Japan



*Speaker

1. Introduction

The current main goal in the field of UHECR (Ultra-High Energy Cosmic Ray) science is to identify their astrophysical sources and composition [1]. For this, increased statistics is one of the essential requirements. A space-based detector for UHECR research has the advantage of a very large exposure and a uniform coverage of the celestial sphere. The aim of the JEM-EUSO program [2] is to bring the study of UHECRs to space. The principle of observation is based on the detection of UV light emitted by isotropic fluorescence of atmospheric nitrogen excited by Extensive Air Showers (EASs) in Earth's atmosphere and forward-beamed Cherenkov radiation reflected at the Earth's surface or at dense cloud tops. The JEM-EUSO program includes missions on ground (EUSO-TA [3]), on stratospheric balloons (EUSO-Balloon [4], EUSO-SPB1 [5], EUSO-SPB2 [6]), and from space (TUS [7], Mini-EUSO [8, 9]) employing fluorescence detectors to demonstrate the feasibility of the UHECR observation from space and prepare for the large size missions K-EUSO [10] and POEMMA [11]. Mini-EUSO is the first detector of the JEM-EUSO program to observe the Earth from the International Space Station (ISS) and to validate from there the observational principle of a space-based detector for UHECR measurements.

2. The Mini-EUSO space telescope

Mini-EUSO (Multiwavelength Imaging New Instrument for the Extreme Universe Space Observatory, known as *UV atmosphere* in the Russian Space Program) [8] is operating on the ISS since October 7th, 2019, and till June 2023, more than 80 sessions have been performed lasting 12 hours each. The pouches containing all stored data are then returned to Earth every ~ 12 months by the Soyuz spacecraft.

The optics are based on two 25 cm diameter Fresnel lenses in Polymethyl methacrylate (PMMA). The Mini-EUSO focal surface, or Photo Detector Module (PDM), consists of a grid of 36 Multi-Anode Photomultiplier Tubes (MAPMTs, Hamamatsu Photonics R11265-M64). Each MAPMT consists of 8×8 pixels, resulting in a total of 2304 channels. The MAPMTs are grouped in Elementary Cells (ECs) of 2×2 MAPMTs. MAPMTs are separated by 2 – 3 mm spacing to avoid vibration damage at launch. Consequently, gaps exist between MAPMTs in the collected images. Each EC has an independent high voltage power supply (HVPS) and board connecting the dynodes and anodes of the four photomultipliers. The HVPS system is based on a Cockroft-Walton circuit. The system has an internal safety mechanism which operates either reducing the collection efficiency of the four MAPMTs or reducing the MAPMT gain when particularly bright signals occur (i.e. lightning or large cities) [8]. The recovery to the nominal mode takes place only few ms after the light level has decreased to a sufficiently low value. In the following we will refer to *Cathode3* for the nominal mode and *Cathode2* for the reduced efficiency/gain mode.

The system has a single photon-counting capability with a double pulse resolution of ~ 6 ns. Photon counts are summed in Gate Time Units (GTUs) of $2.5 \mu\text{s}$. The PDM Data Processor (PDM-DP) stores the $2.5 \mu\text{s}$ GTU data stream (D1) in a running buffer on which the trigger code is executed. A detailed description of the trigger algorithm is reported in [12], which represents an adaptation of the trigger logic conceived for JEM-EUSO [13], while the on-board performance of the trigger system is summarized in [14]. The algorithm searches for a signal integrated over 8

consecutive GTUs above 16 standard deviations from the average in any pixel of the focal surface. The choice to operate on 8 GTUs integration and to act on each pixel independently is based on the time needed by a light signal to cross the FoV of a pixel and the fact that $20 \mu\text{s}$ represent a significant portion of an EAS light-track in atmosphere (see Fig. 1 left).

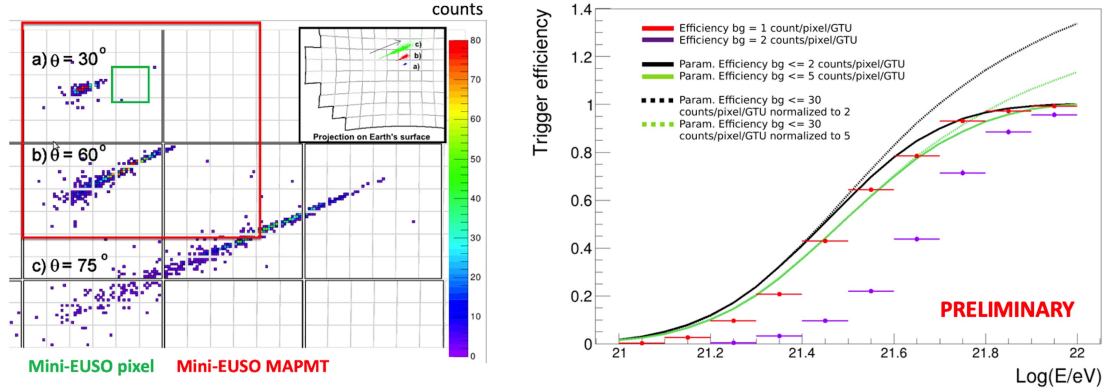


Figure 1: Left: Comparison between JEM-EUSO and Mini-EUSO FoVs. The image shows the detected light track of three simulated EAS with ESAF [15] of energy 10^{20} eV with different zenith angles ($\theta = 30^\circ$, 60° , and 75°) as imaged by JEM-EUSO detector. Each little colored dot represents the pixel FoV of JEM-EUSO projected on ground, each grey square indicates the MAPMT FoV and the large black squares show the FoV of JEM-EUSO PDMs. The green and red squares represent Mini-EUSO pixel's and MAPMT's FoV, respectively. Mini-EUSO pixel's FoV is larger than the FoV of a JEM-EUSO MAPMT and Mini-EUSO MAPMT's FoV is larger than the FoV of one JEM-EUSO PDM. Right: Trigger efficiency curves of Mini-EUSO for ESAF simulated proton-generated EASs of different energies on different background levels. The red and violet points assume a fixed nightglow background of 1 and 2 counts/pix/GTU, respectively. The continuous black (green) line represents the convolved trigger efficiency curve in which each background level below 2 (5) counts/pix/GTU is weighted for the relative fraction of time in which it was measured by Mini-EUSO. The dotted black (green) line provides the fractional increase in exposure [relative to the black (green) line] if the accepted nightglow background is increased from 2 (5) counts/pix/GTU to 30 counts/pix/GTU. A significant increase in exposure is obtained only at the highest energies. See text for details. Image adapted from [16].

Independently from the trigger, sums of 128 frames ($320 \mu\text{s}$, D2) are continuously calculated and stored in another buffer where a similar trigger algorithm, but at this time scale, is running. Similarly, sums of 128 D2 frames (40.96 ms , D3) are calculated in real time and continuously stored. Every 5.24 s , 128 GTUs of D3 data, up to 4 D2 packets and up to 4 D1 packets (if triggers were present) are sent to the CPU for storage. In this way various classes of phenomena with different duration can be detected with an appropriate time scale (see sec. 3 for details).

Prior to the launch, the instrument underwent a series of integration and acceptance tests in Rome, Moscow, and Baikonur, where it was placed in the uncrewed Soyuz capsule. A systematic test of the acquisition logic was performed at the TurLab facility [17] of the University and at the Astrophysical Observatory (INAF-OATo) [18] in Turin. After launch, an end-to-end in-flight calibration of the Mini-EUSO detector has been performed by assembling different UV-flasher systems on ground in Japan, Italy, and France and by firing them in various observational campaigns. A detailed description of the methodology and of the observational results is reported in [19].

3. Mini-EUSO design, expected performance and exposure studies

Mini-EUSO has been designed to detect a photon rate per pixel from diffuse sources (nightglow, clouds, cities, etc.) in the range of values expected from a large mission in space such as the original JEM-EUSO mission [20] or the future detectors K-EUSO or POEMMA. The pixel FoV is, therefore, ~ 100 times larger in area with respect to the FoV of a JEM-EUSO pixel ($\sim 0.5 \times 0.5 \text{ km}^2$), to compensate for the optical system ~ 100 times smaller, constrained by the dimension of the UV transparent window (see Fig. 1 left).

In order to have a precise ratio of the photon rate per pixel from diffuse sources between JEM-EUSO and Mini-EUSO, a full simulation of JEM-EUSO and Mini-EUSO detectors was performed with ESAF simulation software [15]. In case of Mini-EUSO the overall efficiency of the detector was fine-tuned with ESAF, mainly acting at the level of MAPMT response, to match the measured one $\epsilon_{ME} = 0.080 \pm 0.015$ (see the end-to-end in-flight calibration of Mini-EUSO reported in [19]) for a point-like source on ground. A flat diffused UV emission in the range $\lambda = 300 - 400 \text{ nm}$ was simulated at the detector's aperture either with a range of zenith directions much larger than the FoV of the instrument ($\pm 60^\circ$ for both detectors) or just within the FoV of the detectors ($\pm 30^\circ$ for JEM-EUSO and $\pm 22^\circ$ for Mini-EUSO). The estimated background ratio ($R(ME/JE)$) between Mini-EUSO and JEM-EUSO at FS level is $R(ME/JE) = 0.98 - 1.04$ slightly depending on the range of zenith angles. This result confirms that the expected photon rate from diffuse sources is similar in JEM-EUSO and Mini-EUSO instruments.

The energy threshold of Mini-EUSO for point-like sources like UHECRs is roughly 2 orders of magnitude higher than the original JEM-EUSO one. The right side of Fig. 1 shows the trigger efficiency of Mini-EUSO for ESAF simulated proton-generated EASs of different energies. Events have been simulated according to a $\sin(2 \cdot \theta)$ dependence on a larger area than the FoV of the instrument on ground to take into account border effects. The efficiency (ϵ) as a function of the energy (E) has then been calculated as:

$$\epsilon(E) = \frac{N_{trig}}{N_{simu}} \cdot \frac{A_{simu}}{A_{FoV}}, \quad (1)$$

where N_{trig} and N_{simu} represent the number of triggered events over the simulated ones for a specific energy bin, while A_{simu} and A_{FoV} indicate the area on which EAS have been injected and the area on ground in the FoV of Mini-EUSO, respectively. The red and violet points assume a fixed nightglow background of 1 and 2 counts/pix/GTU, respectively. The 50% trigger efficiency is located between $3 - 5 \times 10^{21} \text{ eV}$ depending on the UV nightglow level.

The D3 data taken by Mini-EUSO allow a first comparison with the assumed background levels in JEM-EUSO, K-EUSO and POEMMA to verify that the estimated performance is based on justified assumptions. The analysis presented in the following is preliminary as it is based on part of the data collected in 25 sessions between session 20 and 44. A more refined analysis will be performed when all the data collected by Mini-EUSO is available. The left side of Fig. 2 displays the typical number of minutes in which Mini-EUSO was in operation during all data taking sessions between Session 5 and Session 44. The different time of operation in each orbit reflects several aspects such as the different duration of the night in that specific orbit or the moon condition or the switch on and off by the astronauts among others. The right side of Fig. 2 displays in brown colour

the fraction of time from session 20 to session 44 in which Mini-EUSO operated in a specific Moon Bin (MB). This is compared to the monthly averaged fraction of time in which the Moon appears in the sky with a specific MB (blue colour). Mini-EUSO operated in all the possible Moon conditions with a preference for low Moon phases. This is done on purpose to maximize the scientific potential of Mini-EUSO for atmospheric science (i.e. meteors, elves).

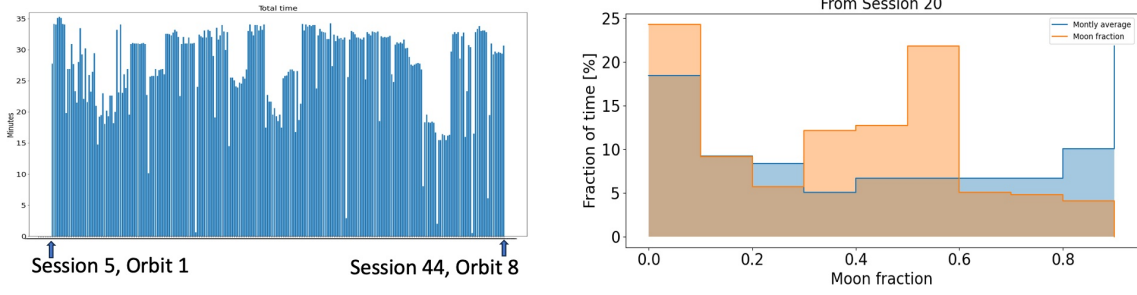


Figure 2: Left: Time in minutes in which Mini-EUSO was operational during the various orbits between session 05 and session 44. Right: Brown histogram displays the fraction of time in which Mini-EUSO was operational between sessions 20 and 44 with a specific MB while blue histogram shows the monthly averaged fraction of time in which the Moon appears in the sky in a specific MB.

According to Mini-EUSO results in low MB conditions, in $\sim 90\%$ of the time of clear sea conditions the count rate is below 2.0 counts/pix/GTU, the median being ~ 0.8 counts/pix/GTU (see Fig. 3). In clear land conditions there is a higher probability of very low counts. These are associated with deserts and forests (see [21] for details). Under the reasonable assumption that conditions above 2 counts/pix/GTU on land are due to the presence of anthropogenic lights ($\sim 20\%$ of the time) and taking into account $\sim 30\%$ land coverage on Earth, this result corresponds to $\sim 6\%$ of the total fraction of time, which is close to the 7% estimation performed for JEM-EUSO in [20]. Moreover, cloudy conditions typically shift curves by a factor 1.5 - 2 towards higher count rates as already measured in JEM-EUSO balloon flights [4]. Taking into account the fact that JEM-EUSO and Mini-EUSO are expected to measure similar count rates from diffuse sources, these results are consistent with the assumption done in [20] for JEM-EUSO where the exposure was calculated under the nominal condition of ~ 1.1 count/pix/GTU.

In order to have a proper estimation of Mini-EUSO exposure at different energies it is necessary to compute an efficiency curve for the various background levels and convolve each efficiency curve with the fraction of time in which such background level is measured. The methodology is described in detail in [16] and we report here only the essential points. As it is not possible to simulate the efficiency curves for infinite background levels, as a first step the efficiency curves are estimated by simulated proton-generated EASs of various energies only for a limited set of background levels in the range [0.2;4.0] counts/pix/GTU and the obtained efficiency curves are fitted with a function of the form:

$$\epsilon(E) = 0.5 \cdot \left[1 + \operatorname{erf} \left(\frac{\log_{10}(E/eV) - P_0}{P_1} \right) \right], \quad (2)$$

where the parameter P_0 indicates the energy (E) at which the efficiency reaches 50% and P_1 measures the slope of the efficiency curve ($\epsilon(E)$). Subsequently, the obtained parameter values at different background levels have been fitted with appropriate functions (logarithmic and exponential

functions for P_0 and P_1 , respectively) and the dependencies of P_0 and P_1 as function of the background level have been obtained. Finally, the trigger efficiency curves are modelled at all background levels by equation (2) using as P_0 and P_1 derived by means of the two functions.

Next, the convolved exposure curve ($\mathcal{E}(E)$) has been calculated according to equation:

$$\mathcal{E}(E) = \sum_i (\epsilon_i(E) \cdot t_i \cdot A_i) \cdot \Omega \cdot t_{tot} \cdot k, \quad (3)$$

where i denotes the UV background level, t_i represents the relative fraction of time in which the measured background is in the interval i (each interval having a width of 0.01 counts/pix/GTU), A_i accounts for the cumulative area on ground with background i , Ω measures the UHECR observational solid angle (which assumes the value of π), and $t_{tot} = 69.16$ hours is the total accumulated time in *Cathode3* mode. The parameter k represents the efficiency factor for detecting the EAS maximum in presence of clouds. This value depends on the type of clouds, their optical depth and height. A detailed analysis was performed at the time of JEM-EUSO and adopted in this calculation ($k = 72\%$).

In order to have a more realistic estimation of the exposure curve, a renormalization has been applied to the fraction of time in which Mini-EUSO has measured a specific UV background level during a specific MB (see left panel of Fig. 3) by rescaling it for the ratio between the fraction of time in which Mini-EUSO operated with a specific MB and the expected monthly average fraction of time according to the Moon cycle (see right panel of Fig. 2). This is summarized in equation:

$$t_i = \sum_{MB} \frac{T_i(MB)}{F(MB)}, \quad (4)$$

where $T_i(MB)$ is the fraction of time in which Mini-EUSO measured the background i in MB and $F(MB)$ is the conversion factor for each MB in order to get the expected monthly averaged fraction of time in a specific MB according to the Moon cycle.

At the same time the duty cycle of Mini-EUSO as a function of the tolerated background level (η_i) can be estimated by the following equation:

$$\eta_i = \frac{1}{\Delta T_{orbit} \cdot N_{orbit}} \cdot \sum_{j=0}^i t_j, \quad (5)$$

and it is displayed in the right panel of Fig. 3. As an example it corresponds to $\eta \sim 15$ (18)% if up to 2 (5) counts/pix/GTU are tolerated to estimate the duty cycle. Finally, the exposure curve obtained by integrating all background levels below 2 (5) counts/pix/GTU has been renormalized using the exposure obtained at the plateau level of 10^{22} eV. The result, which represents the convolved trigger efficiency curve, is shown as black (green) line in Fig. 1. The green curve is very close to the efficiency curve obtained at the fixed background level of 1 count/pix/GTU, indicating that such a curve provides a reasonable approximation of the integrated performance in the various UV background conditions. Moreover, by convolving $\eta = 18\%$ with $k = 72\%$ an effective conversion factor between aperture and exposure of 13% is derived which is consistent with the value obtained in JEM-EUSO computations, confirming the assumptions made in those estimations. Similarly, these conclusions can be extended also to the estimation of K-EUSO and POEMMA trigger efficiency curves as they have been derived adopting the very same methodology used for JEM-EUSO.

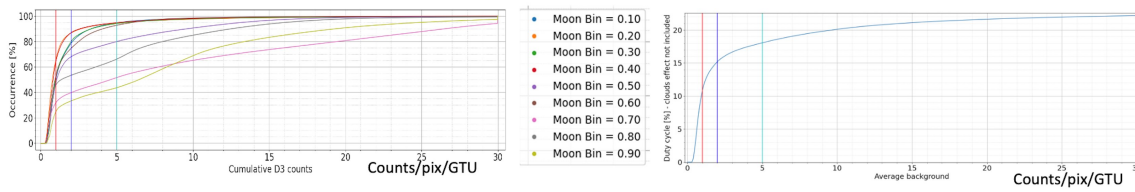


Figure 3: Left: Cumulative fraction of time in which Mini-EUSO measured a UV intensity higher than a specific value reported on the X-axis. Different colours refer to the different MB. Each phase has its own normalization. Right: Same as above but summing up all above distribution each weighted for the expected monthly average fraction of time with a specific MB (see text for details).

The accumulated exposure of Mini-EUSO in this analysis amounts to ~ 1400 Linsley. A very preliminary extrapolation of this result to all good so far recorded data indicates that Mini-EUSO has potentially accumulated till now an exposure equivalent to ~ 3600 Linsley. This value is already about 4% percent of the exposure collected so far by ground-based detectors, and equivalent to the one accumulated in the case of hybrid data [22, 23].

4. Acknowledgements

This work was supported by the Italian Space Agency through the agreement n. 2020-26-Hh.0, by the French space agency CNES, and by the National Science Centre in Poland grants 2017/27/B/ST9/02162 and 2020/37/B/ST9/01821. This research has been supported by the Interdisciplinary Scientific and Educational School of Moscow University “Fundamental and Applied Space Research” and by Russian State Space Corporation Roscosmos. The article has been prepared based on research materials collected in the space experiment “UV atmosphere”. We thank the Altea-Lidal collaboration for providing the orbital data of the ISS.

References

- [1] A. Coleman et al., *Ultra high energy cosmic rays The intersection of the Cosmic and Energy Frontiers, Astroparticle Physics* **149** (2023) 102819 [2205.05845].
- [2] M. Casolino et al., *Overview and latest results of the JEM-EUSO program for the study of ultra-high-energy cosmic-rays from space, This Conf. Proceedings* .
- [3] G. Abdellaoui et al., *EUSO-TA - First results from a ground-based EUSO telescope, Astroparticle Physics* **102** (2018) 98 [1909.09346].
- [4] J.H. Adams Jr. et al., *A Review of the EUSO-Balloon Pathfinder for the JEM-EUSO Program, Space Science Reviews* **218** (2022) 3.
- [5] L. Wiencke, A. Olinto and the JEM-EUSO Coll., *EUSO-SPB1 Mission and Science, PoS(ICRC2017)* **301** (2017) .
- [6] J. Eser et al., *Overview and First Results of EUSO-SPB2, This Conf. Proceedings* .

- [7] P.A. Klimov et al., *The TUS Detector of Extreme Energy Cosmic Rays on Board the Lomonosov Satellite*, *Space Science Reviews* **212** (2017) 1687 [1706.04976].
- [8] S. Bacholle et al., *Mini-EUSO Mission to Study Earth UV Emissions on board the ISS*, *Astrophys. J. Suppl.* **253** (2021) 36 [2010.01937].
- [9] L. Marcelli et al., *Results and performance of the Mini-EUSO telescope on board the ISS*, *This Conf. Proceedings* .
- [10] P.A. Klimov et al., *Status of the K-EUSO Orbital Detector of Ultra-High Energy Cosmic Rays*, *Universe* **8** (2022) 88 [2201.12766].
- [11] A. Olinto et al., *The POEMMA (Probe of Extreme Multi-Messenger Astrophysics) observatory*, *JCAP* **2021** (2021) 007 [2012.07945].
- [12] A. Belov et al., *The integration and testing of the Mini-EUSO multi-level trigger system*, *Advances in Space Research* **62** (2018) 2966 [1711.02376].
- [13] G. Abdellaoui et al., *Cosmic ray oriented performance studies for the JEM-EUSO first level trigger*, *Nucl. Instr. & Meth. A* **866** (2017) 150.
- [14] M. Battisti et al., *Onboard performance of the level 1 trigger of the mini-EUSO telescope*, *Advances in Space Research* **70** (2022) 2750.
- [15] F. Fenu et al., *Simulations for the JEM–EUSO program with ESAF*, *PoS(ICRC2019)* **358** (2019) .
- [16] M. Bertaina et al., *Implications of Mini-EUSO measurements for a space-based observation of UHECRs*, *EPJ Web Conf.* **283** (2023) 06008.
- [17] P. Barrillon et al., *The EUSO@TurLab project in the framework of the JEM-EUSO program*, *Experimental Astronomy* **55** (2023) 569.
- [18] F. Bisconti et al., *Pre-flight qualification tests of the Mini-EUSO telescope engineering model*, *Experimental Astronomy* **53** (2022) 133.
- [19] H. Miyamoto et al., *An end-to-end calibration of the Mini-EUSO detector in space*, *This Conf. Proceedings* .
- [20] J.H. Adams Jr. et al., *An evaluation of the exposure in nadir observation of the JEM-EUSO mission*, *Astroparticle Physics* **44** (2013) 76 [1305.2478].
- [21] M. Casolino et al., *Observation of night-time emissions of the Earth in the near UV range from the International Space Station with the Mini-EUSO detector*, *Remote Sensing of Environment* **284** (2023) 113336 [2212.02353].
- [22] V. Novotný et al., *Energy spectrum of cosmic rays measured using the Pierre Auger Observatory*, *PoS(ICRC2021)* **395** (2021) .
- [23] H. Shin et al., *The measurements of the cosmic ray energy spectrum and the depth of maximum shower development of TA Hybrid trigger events*, *PoS(ICRC2021)* **395** (2021) .

Full Authors list: The JEM-EUSO Collaboration

S. Abe^{ff}, J.H. Adams Jr.^{ld}, D. Allard^{cb}, P. Alldredge^{ld}, R. Aloisio^{ep}, L. Anchordoqui^{le}, A. Anzalone^{ed,eh}, E. Arnone^{ek,el}, M. Bagheri^{lh}, B. Baret^{cb}, D. Barghini^{ek,el,em}, M. Battisti^{cb,ek,el}, R. Bellotti^{ea,eb}, A.A. Belov^{ib}, M. Bertaina^{ek,el}, P.F. Bertone^{lf}, M. Bianciotto^{ek,el}, F. Bisconti^{ei}, C. Blaksley^{fg}, S. Blin-Bondil^{cb}, K. Bolmgren^{ja}, S. Briz^{lb}, J. Burton^{ld}, F. Cafagna^{ea,eb}, G. Cambié^{ei,ej}, D. Campana^{ef}, F. Capel^{db}, R. Caruso^{ec,ed}, M. Casolino^{ei,ej,fg}, C. Cassardo^{ek,el}, A. Castellina^{ek,em}, K. Černý^{ba}, M.J. Christl^{lf}, R. Colalillo^{ef,eg}, L. Conti^{ei,en}, G. Cotto^{ek,el}, H.J. Crawford^{la}, R. Cremonini^{el}, A. Creusot^{cb}, A. Cummings^{lm}, A. de Castro González^{lb}, C. de la Taille^{ca}, R. Diesing^{lb}, P. Dinaucourt^{ca}, A. Di Nola^{eg}, T. Ebisuzaki^{fg}, J. Eser^{lb}, F. Fenu^{eo}, S. Ferrarese^{ek,el}, G. Filippatos^{lc}, W.W. Finch^{lc}, F. Flaminio^{eg}, C. Fornaro^{ei,en}, D. Fuehne^{lc}, C. Fuglesang^{ja}, M. Fukushima^{fa}, S. Gadamsetty^{lh}, D. Gardiol^{ek,em}, G.K. Garipov^{ib}, E. Gazda^{lh}, A. Golzio^{el}, F. Guarino^{ef,eg}, C. Guépin^{lb}, A. Haungs^{da}, T. Heibges^{lc}, F. Isgrò^{ef,eg}, E.G. Judd^{la}, F. Kajino^{fb}, I. Kaneko^{fg}, S.-W. Kim^{ga}, P.A. Klimov^{ib}, J.F. Krizmanic^{lj}, V. Kungel^{lc}, E. Kuznetsov^{ld}, F. López Martínez^{lb}, D. Mandát^{bb}, M. Manfrin^{ek,el}, A. Marcelli^{ej}, L. Marcelli^{ei}, W. Marszał^{ha}, J.N. Matthews^{lg}, M. Mese^{ef,eg}, S.S. Meyer^{lb}, J. Mimouni^{ab}, H. Miyamoto^{ek,el,ep}, Y. Mizumoto^{fd}, A. Monaco^{ea,eb}, S. Nagataki^{fg}, J.M. Nachtman^{li}, D. Naumov^{ia}, A. Neronov^{cb}, T. Nonaka^{fa}, T. Ogawa^{fg}, S. Ogio^{fa}, H. Ohmori^{fg}, A.V. Olinto^{lb}, Y. Onel^{li}, G. Osteria^{ef}, A.N. Otte^{lh}, A. Pagliaro^{ed,eh}, B. Panico^{ef,eg}, E. Parizot^{cb,cc}, I.H. Park^{gb}, T. Paul^{le}, M. Pech^{bb}, F. Perfetto^{ef}, P. Picozza^{ei,ej}, L.W. Piotrowski^{hb}, Z. Plebaniak^{ei,ej}, J. Posligual^{li}, M. Potts^{lh}, R. Prevede^{ef,eg}, G. Prévôt^{cb}, M. Przybylak^{ha}, E. Reali^{ei,ej}, P. Reardon^{ld}, M.H. Reno^{li}, M. Ricci^{ee}, O.F. Romero Matamala^{lh}, G. Romoli^{ei,ej}, H. Sagawa^{fa}, N. Sakaki^{fg}, O.A. Saprykin^{ic}, F. Sarazin^{lc}, M. Sato^{fe}, P. Schovánek^{bb}, V. Scotti^{ef,eg}, S. Selmane^{cb}, S.A. Sharakin^{ib}, K. Shinozaki^{ha}, S. Stepanoff^{lh}, J.F. Soriano^{le}, J. Szabelski^{ha}, N. Tajima^{fg}, T. Tajima^{fg}, Y. Takahashi^{fe}, M. Takeda^{fa}, Y. Takizawa^{fg}, S.B. Thomas^{lg}, L.G. Tkachev^{ia}, T. Tomida^{fc}, S. Toscano^{ka}, M. Traïche^{aa}, D. Trofimov^{cb,ib}, K. Tsuno^{fg}, P. Vallania^{ek,em}, L. Valore^{ef,eg}, T.M. Venters^{lj}, C. Vigorito^{ek,el}, M. Vrubel^{ha}, S. Wada^{fg}, J. Watts Jr.^{ld}, L. Wiencke^{lc}, D. Winn^{lk}, H. Wistrand^{lc}, I.V. Yashin^{ib}, R. Young^{lf}, M.Yu. Zotov^{ib}.

^{aa} Centre for Development of Advanced Technologies (CDTA), Algiers, Algeria

^{ab} Lab. of Math. and Sub-Atomic Phys. (LPMPs), Univ. Constantine I, Constantine, Algeria

^{ba} Joint Laboratory of Optics, Faculty of Science, Palacký University, Olomouc, Czech Republic

^{bb} Institute of Physics of the Czech Academy of Sciences, Prague, Czech Republic

^{ca} Omega, Ecole Polytechnique, CNRS/IN2P3, Palaiseau, France

^{cb} Université de Paris, CNRS, AstroParticule et Cosmologie, F-75013 Paris, France

^{cc} Institut Universitaire de France (IUF), France

^{da} Karlsruhe Institute of Technology (KIT), Germany

^{db} Max Planck Institute for Physics, Munich, Germany

^{ea} Istituto Nazionale di Fisica Nucleare - Sezione di Bari, Italy

^{eb} Università degli Studi di Bari Aldo Moro, Italy

^{ec} Dipartimento di Fisica e Astronomia "Ettore Majorana", Università di Catania, Italy

^{ed} Istituto Nazionale di Fisica Nucleare - Sezione di Catania, Italy

^{ee} Istituto Nazionale di Fisica Nucleare - Laboratori Nazionali di Frascati, Italy

^{ef} Istituto Nazionale di Fisica Nucleare - Sezione di Napoli, Italy

^{eg} Università di Napoli Federico II - Dipartimento di Fisica "Ettore Pancini", Italy

- eh* INAF - Istituto di Astrofisica Spaziale e Fisica Cosmica di Palermo, Italy
- ei* Istituto Nazionale di Fisica Nucleare - Sezione di Roma Tor Vergata, Italy
- ej* Università di Roma Tor Vergata - Dipartimento di Fisica, Roma, Italy
- ek* Istituto Nazionale di Fisica Nucleare - Sezione di Torino, Italy
- el* Dipartimento di Fisica, Università di Torino, Italy
- em* Osservatorio Astrofisico di Torino, Istituto Nazionale di Astrofisica, Italy
- en* Uninettuno University, Rome, Italy
- eo* Agenzia Spaziale Italiana, Via del Politecnico, 00133, Roma, Italy
- ep* Gran Sasso Science Institute, L'Aquila, Italy
- fa* Institute for Cosmic Ray Research, University of Tokyo, Kashiwa, Japan
- fb* Konan University, Kobe, Japan
- fc* Shinshu University, Nagano, Japan
- fd* National Astronomical Observatory, Mitaka, Japan
- fe* Hokkaido University, Sapporo, Japan
- ff* Nihon University Chiyoda, Tokyo, Japan
- fg* RIKEN, Wako, Japan
- ga* Korea Astronomy and Space Science Institute
- gb* Sungkyunkwan University, Seoul, Republic of Korea
- ha* National Centre for Nuclear Research, Otwock, Poland
- hb* Faculty of Physics, University of Warsaw, Poland
- ia* Joint Institute for Nuclear Research, Dubna, Russia
- ib* Skobeltsyn Institute of Nuclear Physics, Lomonosov Moscow State University, Russia
- ic* Space Regatta Consortium, Korolev, Russia
- ja* KTH Royal Institute of Technology, Stockholm, Sweden
- ka* ISDC Data Centre for Astrophysics, Versoix, Switzerland
- la* Space Science Laboratory, University of California, Berkeley, CA, USA
- lb* University of Chicago, IL, USA
- lc* Colorado School of Mines, Golden, CO, USA
- ld* University of Alabama in Huntsville, Huntsville, AL, USA
- le* Lehman College, City University of New York (CUNY), NY, USA
- lf* NASA Marshall Space Flight Center, Huntsville, AL, USA
- lg* University of Utah, Salt Lake City, UT, USA
- lh* Georgia Institute of Technology, USA
- li* University of Iowa, Iowa City, IA, USA
- lj* NASA Goddard Space Flight Center, Greenbelt, MD, USA
- lk* Fairfield University, Fairfield, CT, USA
- ll* Department of Physics and Astronomy, University of California, Irvine, USA
- lm* Pennsylvania State University, PA, USA